Pore scale investigation of unsaturated granular soil behaviour by means of *in situ* CT experiments

Marius Milatz[1*] and *Dennis* Heinrich[1]

[1]Hamburg University of Technology, Institute of Geotechnical Engineering and Construction Management, 21079 Hamburg, Germany

Abstract. With continuing evolution of imaging techniques from medical applications and materials science, non-destructive imaging experiments have also become an important method to investigate soil specimens. Amongst other methods, computed tomography (CT) has developed to a tool to visualise and better understand the microstructure of different soils based on 3D image data. Furthermore, the acquisition of a temporal series of CT images allows to study processes in soils on the microscale, *e. g.*, during mechanical loading. In order to study the hydraulic and mechanical behaviour of unsaturated granular soils, we combine different custom-built miniaturised experimental set-ups with geomechanics background with computed tomography, yielding so-called *in situ* CT experiments. By means of image reconstruction and further image analysis based on segmented CT images acquired during different hydraulic and mechanical experiments, we study the drainage and imbibition process as well as the shear process of unsaturated sand and glass bead specimens on the pore or grain scale. The analysis of data on the microscopic level, including the phase distribution, interfacial areas, contact lines as well as radii of curvature of capillary menisci, allows to obtain insights into the macroscopic water retention behaviour and shear behaviour of granular soils.

1 Introduction

1.1 Aims of research

In order to better understand the macroscopic soil behaviour of unsaturated granular soils governed by the acting of capillary effects, it is worth studying the capillary interaction of pore water and pore air with the soil grains on a grain or pore scale. By means of soil mechanical experiments run in a CT scanning environment, so-called *in situ* CT experiments, we intend to quantitatively measure and analyse the change of capillary effects in unsaturated sandy soils. The capillary effects are quantified on the pore scale by means of so-called *capillary state variables* which include fluid clusters (water and air volumes), representing the local pore-scale phase distribution, their interfacial (surface) areas, their contact lines as well as contact angles and radii of curvature which represent wettability and the link to capillary pressure. In different miniaturised experiments, the afore mentioned capillary state variables are measured based on image data and analysed regarding their change during hydraulic and mechanical processes. An attempt is made to link the local microscopic pore scale hydro-mechanical behaviour to the macroscopic soil response as given by the water retention curve (WRC) as well as shear strength and volume change behaviour upon mechanical loading.

1.2 Unsaturated soil mechanics on the pore scale

Different previous works have applied CT to study the behaviour of unsaturated soils. The WRC related to pore scale phase distributions has been studied by means of laboratory X-ray CT by several authors [1–3]. Furthermore, scientists have applied synchrotron-based CT to study flow processes in geomaterials [4–6]. Especially the spatially and temporarily highly resolved CT images at the synchrotron allow to study interfacial areas [4] as well as pore filling and emptying processes [5] and relate the pore scale findings to macroscopic capillary pressure [6]. Other authors have focused on the hydromechanical coupling in unsaturated soils and have studied their shear behaviour by means of triaxial tests in a CT scanner [7–10]. By analysing the evolution of the pore water distribution as well as fluid clusters, the influence of shearing on capillary state variables such as liquid clusters could be studied.

The key to obtain pore scale insights from CT data is a good image quality at a high signal-to-noise ratio combined with appropriate image processing steps allowing to segment, *i. e.*, to separate, images into different constituent phases. For the segmentation process, different tools and algorithms have been presented that are described in the corresponding literature, *e. g.*, [11].

Based on volumetric image data segmented into different phases, different capillary state variables can

* Corresponding author: marius.milatz@tuhh.de

be defined and extracted to describe local state changes within soil specimens and to link them to the macroscopic soil behaviour. Within the scope of this paper, the air and water phase distributions as well as the air-water interfacial area a^{nw} and the solid-water interfacial area a^{sw} are extracted from images as described in [12, 13]. While the phase distributions correspond to the degree of saturation S_r inside of the specimen, defined as the ratio of pore space occupied by pore water to the pore space inside a reference volume either defined as a single pore or as the whole soil volume, the interfacial areas reflect geometric zones of capillary action. The air-water interfacial area a^{nw} represents the surface area of menisci, transferring surface tension, whereas the solid-water interfacial area a^{sw} directly reflects the amount of wetted surface area of soil grains. It is this area through which capillary pressure acts in between the soil grains. Both, surface tension and capillary pressure, lead to a significant contribution to effective stress in unsaturated soils which is why the corresponding interfacial areas might be used as descriptors for effective stress, *e. g.* [14–16].

Wettability is the affinity of a granular medium's surface to be covered by liquids. Recently, this property has been focused on as an important measure to describe multiphase fluid flow on the pore level in unsaturated porous media [17, 18]. Wettability is mainly described by the contact angle θ between the wetting phase (in this case pore water) and the soil grain surface. The contact angle forms around the so-called triphase or contact line, another pore scale capillary state variable, geometrically represented by the 3D line linking all three present phases, air, water, and solid. Both, the contact line and contact angles, can be determined from 3D images following different approaches [17, 18]. Besides contact angles, also radii of curvature of capillary menisci can be measured. Using the Young-Laplace equation, the radii of curvature can be applied to compute local capillary pressure, with the macroscopic capillary pressure apparently depending on the statistical distribution of local radii of curvatures [6].

In addition to the fluid phases, also changes of the grain skeleton can be studied based on CT image data, *e. g.*, using *discrete digital image correlation* (DDIC) techniques [19]. By means of tracking soil grains, their displacements, rotations and contacts properties in 3D images, the evolution of the grain skeleton and its fabric can be quantitatively measured during mechanical loading.

2 Material and methods

2.1 CT experiments

Running *in situ* CT experiments requires miniaturised experimental set-ups and a suitable CT scanning environment. For research on granular media, laboratory CT systems, consisting of an X-ray source, a rotation stage, and a detector are used [20].

Typically, the experimental set-ups are fitted onto the rotation stage and are operated remotely, applying load or flow steps to the studied soil specimens, while tomographies are acquired at regular time or loading steps. A special challenge is the design of miniaturised set-ups that can be remote-controlled. A fruitful approach is the use of *single-board computers* to design custom-built experimental environments to study unsaturated granular soils, *e. g.*, as described in [21].

Depending on the speed of the studied physical process as well as acquisition time required to gather CT data at a desired resolution in a selected field of view of the specimen, the loading process is either halted for imaging or the imaging process is run continuously during loading. The second option is frequently selected if synchrotron-based X-ray radiation is applied at synchrotron radiation research facilities which allow a temporarily and spatially highly resolved imaging thanks to the brilliance of synchrotron-based X-rays [11]. Besides X-rays, also neutron radiation can be applied for imaging of geomaterials, yielding an enhanced selective contrast for pore water as compared to X-rays [22].

Within the scope of this paper, we focus on different set-ups for in situ CT imaging of pore scale flow and shear processes of unsaturated granular media, such as sand and glass beads, with the latter material representing a model soil with ideal spherical grains. Selected properties of the studied granular materials are summarised in Table 1. While Hamburg Sand is a medium coarse to coarse grained natural quartz sand, the soda-lime glass beads represent a polydisperse bead mixture, approximating the grain size distribution of Hamburg Sand. More material-specific information is given in [12].

Table 1. Properties of the studied granular materials. ρ_s: grain density, e_{min}: min. void ratio, e_{max}: max. void ratio, d_{10}: grain diameter at 10% passing, d_{50}: grain diameter at 50% passing, d_{max}: max. grain diameter

Hamburg Sand					
ρ_s	e_{min}	e_{max}	d_{10}	d_{50}	d_{max}
[g/cm³]	[-]	[-]	[mm]	[mm]	[mm]
2.64	0.52	0.805	0.45	0.68	2.0
Glass beads ("Hamburg Glass")					
ρ_s	e_{min}	e_{max}	d_{10}	d_{50}	d_{max}
[g/cm³]	[-]	[-]	[mm]	[mm]	[mm]
2.50	0.555	0.679	0.45	0.68	1.3

2.2 *In situ* flow experiments

In order to study the water retention behaviour in unsaturated air- and water-filled soil specimens on the pore level by means of *in situ* CT flow experiments, a miniaturised flow cell apparatus has been designed [21] and applied using laboratory X-ray CT imaging [13] as well as sychrotron-based CT imaging at the German Synchrotron Radiation Facility Deutsches Elektronen-Synchrotron (DESY) in Hamburg. In the framework of this paper, we focus on the experiments using the laboratory CT scanner at Laboratoire 3SR, Université Grenoble Alpes [20]. With the aim to investigate possible pore scale origins of hysteresis of the macroscopic water retention curve, cyclic drainage and imbibition steps were applied to an initially water-saturated Hamburg Sand specimen. The degree of

saturation was changed linearly and cyclically over time at a constant flow rate of pore water through a porous base pedestal of the specimen by means of a syringe pump. Simultaneously, matric suction was measured as a response using a tensiometer in the pore water drainage system [13]. 3D tomographies were acquired on different hydraulic paths of the macroscopic WRC to analyse differences in pore scale capillary state variables.

2.3 *In situ* shear tests

Based on the early design of miniaturised uniaxial compression apparatus [12] to study the shear behaviour of unsaturated granular soil columns under uniaxial compression, the shear process has been further focused on in different new apparatuses. Besides improvements made on the uniaxial compression apparatus [23], a miniaturised prototype direct shear apparatus has been designed. In this paper, we focus on uniaxial compression tests on unsaturated Hamburg Sand and glass beads with laboratory X-ray CT imaging run at Laboratoire 3SR in Grenoble and on direct shear tests on sand with synchrotron-based CT imaging run at the synchrotron DESY in Hamburg. In all shear tests, the dry granular materials were initially mixed with de-ionised water to establish a selected initial degree of saturation S_{r0} at a given initial void ratio e_0. Afterwards, the specimens were sheared with displacement-control, with full-field tomographies being captured initially and for selected loading steps with shear loading halted.

3 Experimental results

The experimental results presented in this section are based on "4D data", *i. e.*, temporal 3D image data with time being the fourth dimension. After image acquisition, the greyscale images are filtered to improve image quality and then segmented to split up the data into air, water, and solid volumes. The segmented image data is the basis for further image analysis steps, *e. g.*, the extraction of interfacial areas, the measurement of contact angles or DDIC analyses using the open-source software *spam* [19] to measure grain displacements, strain distributions and pore-based degree of saturation. The image processing and analysis steps are described in detail in [12] and [13].

3.1 Unsaturated flow on the pore scale

The macroscopic WRC measured in an *in situ* CT experiment on Hamburg Sand is shown in Figure 1. The black horizontal lines represent the drift of continuously measured suction with flow halted during CT imaging steps. The WRC shows pronounced hysteresis with elliptical paths measured for drainage and imbibition cycles. Furthermore, the suction measurements show strong oscillations on drainage paths, especially for primary drainage, while the suction data is smoother on imbibition paths. During CT imaging, the suction measurements show a slight drift, revealing an "overshooting" on drainage paths and an "under-shooting" on imbibition paths. This behaviour is due to the transient nature of the studied WRC which is measured continuously at a constant flow rate of 0.0597 mm³/s leading to small non-equilibrium effects.

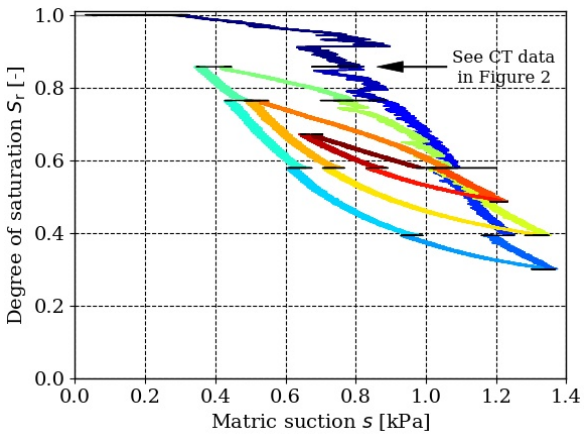

Fig. 1. Macroscopic WRC measured during an *in situ* CT-experiment on Hamburg Sand. Different consecutive drainage and imbibition paths are coloured from cold (blue) to warm (red). Black data are recorded during CT imaging steps with flow halted.

By studying the phase distribution, highlighted in Figure 2 for the first CT scan on the primary drainage path, the macroscopic WRC can be linked to local flow events on the pore level.

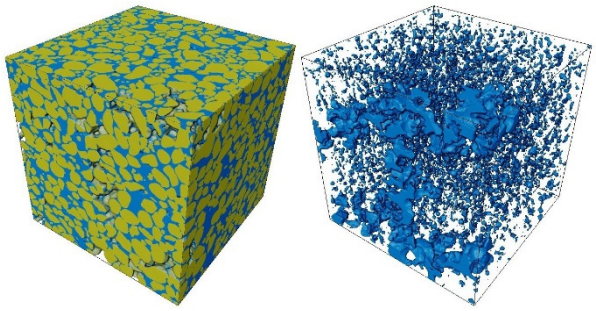

Fig. 2. Segmented CT data in a central cubic subvolume with edge length of 8 mm at a voxel size of 10 µm after the first primary drainage step (indicated in Figure 1). Left: sand and water phase; right: air phase only, revealing a vertical air channel entering from top.

The evolution of the air phase, entering from the specimen top into the pores in discrete channels, confirms the so-called *Haines jumps* upon drainage These jumps and oscillations of suction measured for primary drainage can be shown to be related to sudden air fingering into initially water-filled pores.

Beyond the phase distribution, specific interfacial areas (per unit volume) are measured for different hydraulic states to study their evolution on different hydraulic cycles. The air-water (a^{nw}) and solid-water (a^{sw}) interfacial areas in Figure 3 are extracted after air entry on the primary drainage path. The areas represent the surfaces of action of surface tension in the case of a^{nw} and of capillary pressure in the case of a^{sw}. If the individual surfaces are measured for all available hydraulic steps and plotted either *vs.* suction or degree of saturation, characteristic relationships are revealed [13], which show pronounced hysteresis when plotted

vs. suction, see Figure 4. Due to their meaning for capillary action, the interfacial areas might be used as capillary state variables for new effective stress formulations in unsaturated soils. Furthermore, they might help to better understand hydraulic hysteresis of the WRC.

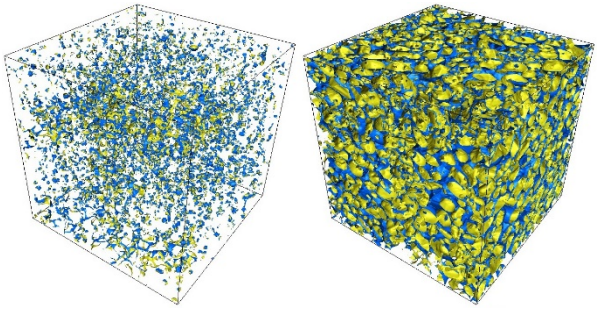

Fig. 3. Extracted air-water interfacial area a^{nw} (left) and solid-water interfacial area a^{sw} (right) in a central cubic subvolume with edge length of 8 mm after the first primary drainage step (indicated in Figure 1).

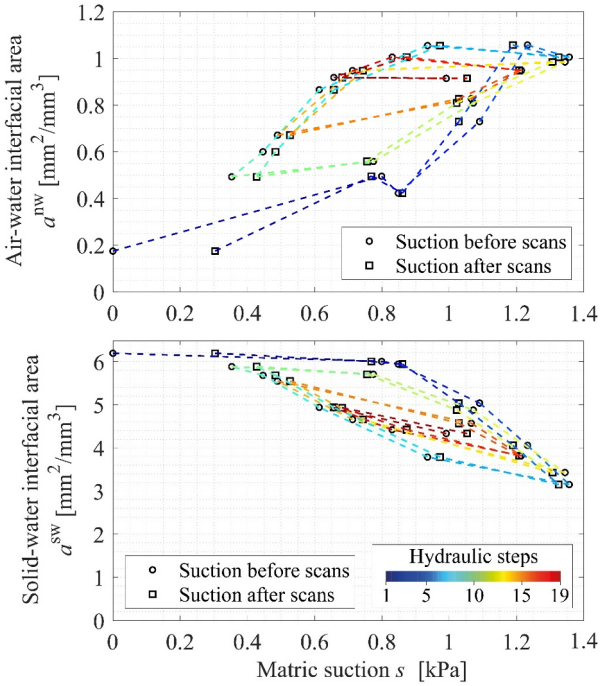

Fig. 4. Evolution of air-water interfacial area a^{nw} (top) and solid-water interfacial area a^{sw} (bottom) in a central cubic subvolume with edge length of 8 mm plotted *vs.* measured macroscopic matric suction.

Figure 5 (top) shows the evolution of contact angles measured manually for all 19 hydraulic steps [13]. Despite the scatter in the data, the mean contact angle shows differences between drainage and imbibition contact angles with a smooth transition of wettability for changes in flow direction. The mean contact angle is higher on imbibition paths as compared to drainage paths. This *contact angle hysteresis* is believed to be one source for hysteresis of the macroscopic WRC. Also the radii of curvature R_1 in Figure 5 (bottom) measured from 2D images show hysteresis with their mean being larger on imbibition paths as compared to drainage paths.

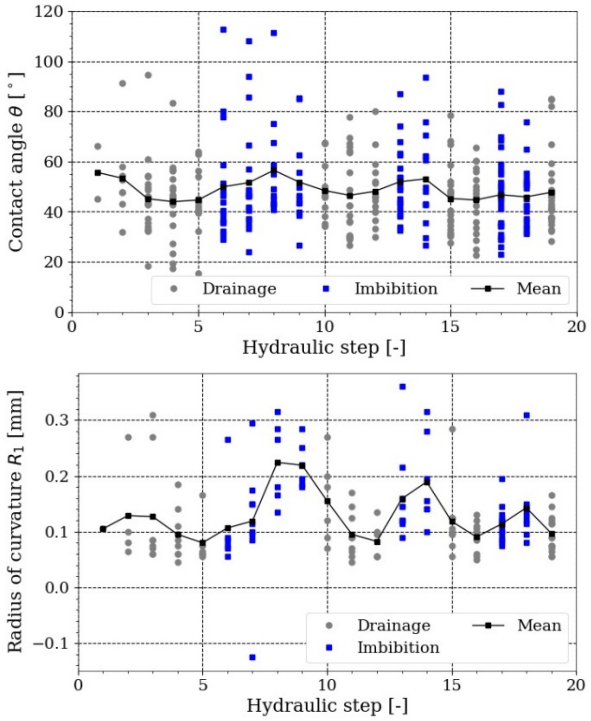

Fig. 5. Measured contact angles (top) and 2D-radii of curvature (bottom) *vs.* hydraulic steps on drainage and imbibition paths.

Using the Young-Laplace equation and the surface tension of water $\gamma = 0.07275$ N/m at 20°C, capillary pressure p_c (suction) can be computed from γ/R_1, neglecting the contribution of the second radius of curvature R_2 for 2D conditions [13]. A comparison of computed capillary pressures, their mean and macroscopic capillary pressure (suction) measured before and after each CT scan are compared in Figure 6. Interestingly, the mean capillary pressure obtained from radii of curvature measured in CT images is close to the macroscopic capillary pressure, revealing the local radii of curvature as important capillary state variables, representing the macroscopic capillary pressure state.

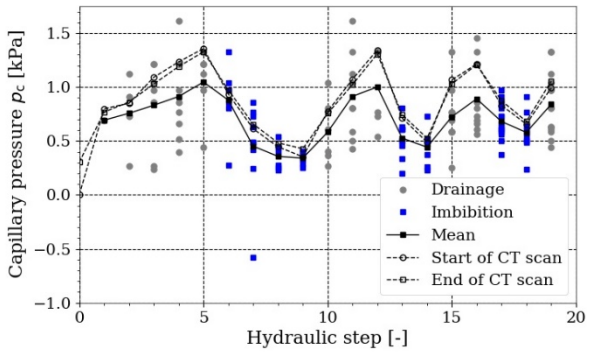

Fig. 6. Measured macroscopic capillary pressure (suction) at start and end of a CT scan compared to capillary pressures and their mean value computed from 2D radii of curvature *vs.* hydraulic steps on drainage and imbibition paths.

3.2 Shearing of unsaturated granular media on the grain scale

By means of uniaxial compression tests on unsaturated soil columns ($h = d = 12$ mm) without lateral confinement, the increase in shear strength due to

capillary interactions and their effect on volume change have been studied [12]. Figure 7 shows the pre and post shear state of Hamburg Sand (e_0 = 0.631, S_{r0} = 0.212) and glass beads (e_0 = 0.567, S_{r0} = 0.325). Despite an axial straining exceeding ε = 0.15, the grain skeleton in both materials was found to stay intact without a loss of single particles due to adhesion caused by capillary bridges and liquid clusters. As compared to the glass beads, Hamburg Sand shows a much higher shear strength and a more pronounced dilatant volumetric behaviour [12].

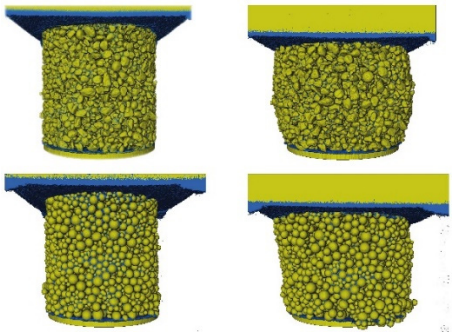

Fig. 7. Segmented CT data at a voxel size of 11 µm measured during uniaxial compression of unsaturated Hamburg Sand (top row) and glass bead columns (bottom row). Images on the right indicate the post shear state after six shear steps.

Similar to the previously discussed hydraulic experiments, interesting findings on the hydro-mechanical coupling are obtained by studying the liquid phase during the shear process. Figure 8 shows individual liquid clusters of different sizes labelled in different colours. A separate cluster is identified as a set of neighbouring voxels at least being connected at a common vertex. Water clusters show a more regular shape in glass beads as compared to sand. In both materials, the shearing leads to the straining and rupture of water clusters. Initially larger present water clusters disintegrate into smaller ones, especially in shear zones, while small clusters and liquid bridges appear to remain intact. A deeper analysis of this behaviour is presented in [12]. The change of capillary bonds due to mechanical loading seems to be a characteristic trait of hydro-mechanical coupling in unsaturated granular soils and its meaning for shear strength should be further studied in future experiments.

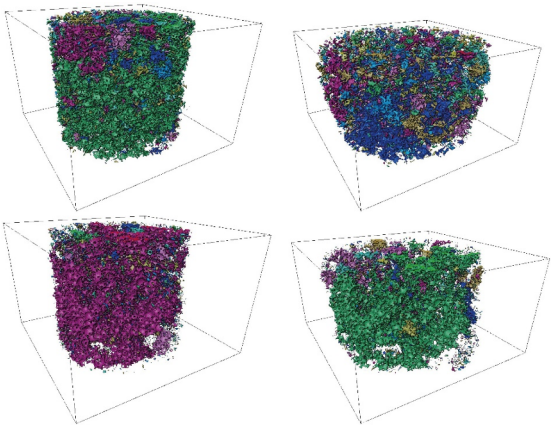

Fig. 8. Segmented and labelled water clusters measured during uniaxial compression of unsaturated Hamburg Sand (top row) and glass bead columns (bottom row). Images on the right indicate the post shear state after six shear steps.

The mechanical effect of capillary bridges and liquid clusters is also highlighted by the evolution of mean coordination number in Figure 9 measured on labelled images of solid grains tracked by DDIC for all uniaxial compression steps on both materials. Due to dilatancy, the coordination number is reduced in both materials. This average loss of contact partners is especially pronounced in the sand, probably due to strong grain rotations and opening of pores, but the grain skeleton remains stable due to capillary bonding of grains.

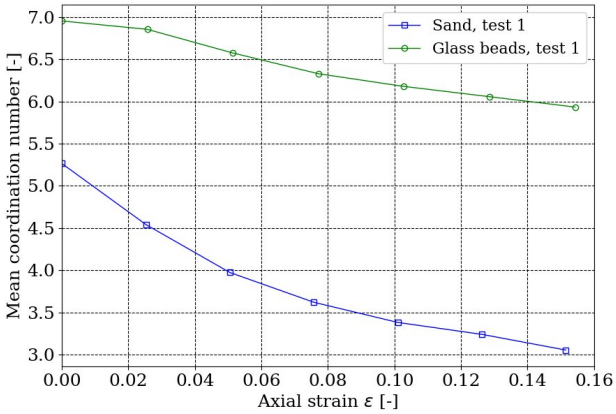

Fig. 9. Evolution of mean coordination number derived from CT data measured during uniaxial compression of unsaturated Hamburg Sand and glass bead columns [12].

Further first insights into the shear behaviour of unsaturated granular materials have been obtained by means of miniaturised direct shear tests with parallel synchrotron-based CT imaging, allowing for a temporal resolution of ca. 10 min and a spatial resolution of 2.56 µm. The experimental set-up imaged at DESY's P07 High Energy Materials Science Beamline is presented in Figure 10, showing the hardware of the direct shear apparatus on the rotation stage with detail of the sheared specimen and the imaged field of view of ca. 6.57 mm × 5.02 mm, centred around the shear zone.

A glimpse into direct shearing of Hamburg Sand on the pore scale inside of the shear plane is given in Figure 11. During stepwise horizontal displacement of the lower shear box compartment, individual grains are observed to rotate and move upward causing a dilatant increase of specimen height on the macro level, while locally capillary bridges are deforming, breaking and reordering around moving grains.

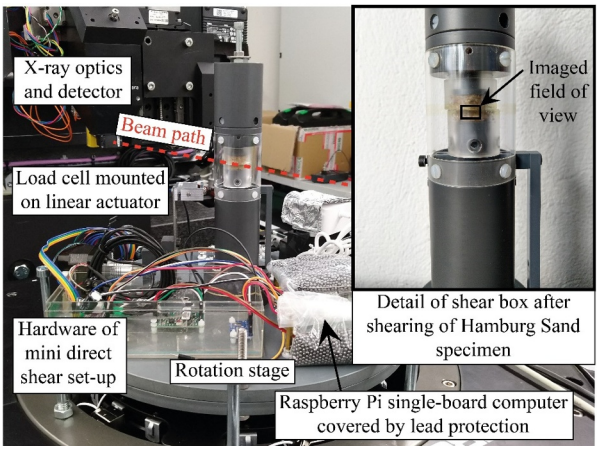

Fig. 10. Miniaturised direct shear set-up for synchrotron-based CT imaging of direct shearing of unsaturated Hamburg Sand.

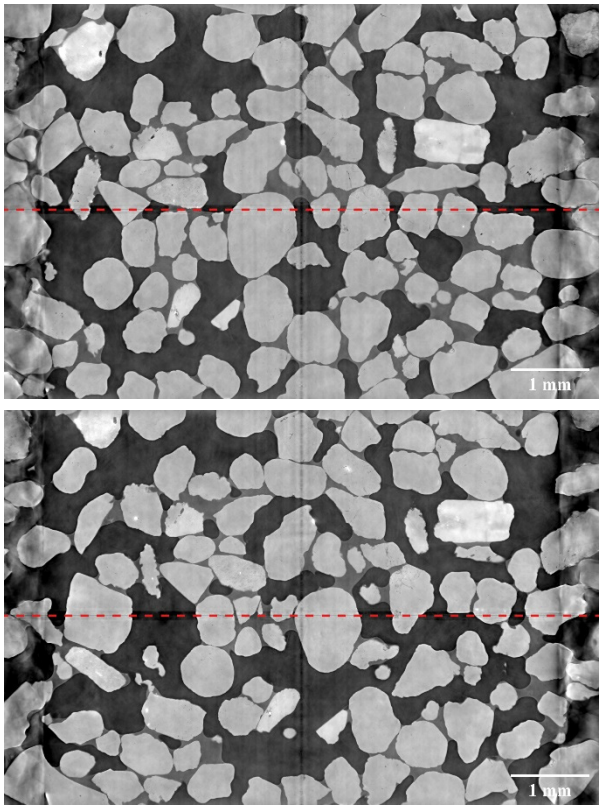

Fig. 11. Vertical slices through an unsaturated Hamburg Sand specimen subjected to direct shearing (shear direction from left to right). The dashed horizontal line in the middle indicates the enforced shear plane. Top: initial state, bottom: post shear state after ten shear steps with an individual increment of 0.2 mm.

4 Conclusion and outlook

By means of *in situ* CT experiments on soil specimens and an elaborated analysis of micro structures and their change on the pore level during hydraulic or mechanical loading, links to the macroscopic soil behaviour can be established. In the case of unsaturated granular soils, pore scale flow processes, phase distributions, and capillary structures can be shown to be responsible for the macroscopic water retention behaviour as well as shear strength.

In the future, the presented experimental set-ups will be further refined and used in conjunction with higher spatial and temporal resolutions. In the case of the direct shear test, changes in the capillary state inside and outside of the shear zone will be studied in more detail as well as grain kinematics influenced by capillarity.

The funding of this work by the German Research Foundation (Deutsche Forschungsgemeinschaft, DFG) in the framework of Research Training Group GRK 2462 “Processes in natural and technical Particle-Fluid-Systems (PintPFS)” is greatly acknowledged. The authors also thank the beamline scientists at Deutsches Elektronen-Synchrotron (DESY) for their support during beamtime I-20210425.

References

1. Y. Higo, R. Morishita, R. Kido, G. Khaddour, S. Salager, Jpn. Geotech. Soc. spec. publ., **2**(16), 635–638 (2015)
2. G. Khaddour, I. Riedel, E. Andò, P. Charrier, P. Bésuelle, J. Desrues, G. Viggiani, S. Salager, Acta Geotech., **13**, 497–512 (2018)
3. R. Kido, Y. Higo, F. Takamura, R. Morishita, G. Khaddour, Acta Geotech., **15**, 1745–1761 (2020)
4. K. A. Culligan, D. Wildenschild, B. S. B. Christensen, W. G. Gray, M. L. Rivers, A. F. B. Tompson, Water Resour. Res., **40**, W12413 (2004)
5. S. Schlüter, S. Berg, M. Rücker, R. T. Armstrong, H.-J. Vogel, R. Hilfer, D. Wildenschild, Water Resour. Res., **52**(3), 2194–2205 (2016)
6. R. T. Armstrong, M. L. Porter, D. Wildenschild, Adv. Water Resour., **46**, 55–62 (2012)
7. Y. Higo, F. Oka, T. Sato, Y. Matsushima, S. Kimono, Soils Found., **53**(2), 181–198 (2013)
8. G. Khaddour, Ph. D. thesis. Laboratoire 3SR, Univ. Grenoble Alpes (2015)
9. R. Kido, Y. Higo, Acta Geotech., **15**, 3055–3073 (2020)
10. J.-P. Wang, J.-Y. Luan, X.-G. Gao, T.-H. Liu, E. Andò, B. François, Acta Geotech., **17**, 4799–4821 (2022)
11. D. Wildenschild, A. P. Sheppard, Adv. Water Resour., **51**, 217–246 (2013)
12. M. Milatz, N. Hüsener, E. Andò, G. Viggiani, J. Grabe, Acta Geotech., **16**, 3573–3600 (2021)
13. M. Milatz, E. Andò, G. Viggiani, S. Mora, Open Geomech., **3**, article no. 5 (2022)
14. W. G. Gray, B. A. Schrefler, F. Pesavento, J. Mech. Phys. Solids, **57**, 539–554 (2009)
15. E. Nikooee, G. Habibagahi, S. M. Hassanizadeh, A. Ghahramani, Transp. Porous Media, **96**, 369–396 (2013)
16. J. Wang, P. Lambert, T. De Kock, V. Cnudde, B. François, Acta Geotech., **14**, 1545–1559 (2019)
17. A. AlRatrout, A. Q. Raeini, B. Bijeljic, M. J. Blunt, Adv. Water Resour., **109**, 158–169 (2017)
18. A. Mascini, V. Cnudde, T. Bultreys, J. Colloid Interface Sci., **572**, 354–363 (2020)
19. O. Stamati *et al.*, J. Open Source Softw., **5**(51), 2286 (2020)
20. G. Viggiani, E. Andò, E. Takano, J. C. Santamarina, Geotech. Test. J., **38**(1), 61–71 (2015)
21. M. Milatz, Acta Geotech., **15**, 2239–2257 (2020)
22. A. Tengattini, N. Lenoir, E. Andò, G. Viggiani, Geomech. Energy Environ., **27**, 100206 (2021)
23. D. Heinrich, M. Milatz, TUHH Open Research (TORE), DOI: 10.15480/336.4393 (2022)